AES and XPS Analysis of Nanowear and Thin Films

J. T. Grant
Research Institute, University of Dayton, 300 College Park, Dayton, Ohio, 45469-0168, USA.
j.grant@ieee.org
(Received; Feb 21, 2002)

Auger electron spectroscopy (AES) and X-ray photoelectron spectroscopy (XPS/ESCA) have been used to characterize a variety of samples, including those related to micro electro mechanical systems (MEMS) and to industrial needs. The relatively high spatial resolution of AES is very useful for the surface compositional analysis of MEMS devices and can often provide information about surface chemistry as well. Where spatial resolution limitations are not a problem, XPS usually provides superior quantitative analysis as well as superior chemical information of the surface composition.

1. Introduction

Auger electron spectroscopy (AES) and X-ray photoelectron spectroscopy (XPS), (XPS is also often referred to as ESCA, electron spectroscopy for chemical analysis), are commonly used techniques for determining the surface composition of materials. The spatial resolution of these instruments has improved over the years, with state of the art commercial instruments being able to acquire spectra from areas of the order of 50 nm (AES) and 10 μm (XPS). With AES, regions to be analyzed are determined by operating the instrument in the SEM mode and measuring the secondary electrons or backscattered electrons leaving the sample, or by measuring changes in the current to ground as the electron beam is rastered on the sample. With XPS, regions to be analyzed are located by (previously calibrated) optical microscopes, video cameras, x-ray induced electron emission, or by imaging the sample through the analyzer using an electron beam. Higher spatial resolutions with XPS can be achieved by conducting the analysis at a synchrotron, where spatial resolutions of the order of 100 nm can be achieved. The main purpose of this symposium is to focus on the potentiality and present status of various surface analysis techniques for nano-materials and/or industrial applications, and this paper will give some examples of the application of AES and XPS to study nanowear, MEMS devices, thin films and industrial samples.

2. Equipment

Two different instruments were used for the analyses reported here. A Physical Electronics Inc (PHI) model 5700 AES/XPS system was used for the AES analyses, and a Surface Science Instruments (SSI) M-Probe was used for most of the XPS analyses. The electron gun on this PHI system has a minimum electron beam diameter of 100 nm at 10 keV beam energy when measuring the signal levels across a grid. Secondary electrons were used for imaging the sample surface. The highest spatial resolution of the SSI XPS is 150 μm, with the maximum analysis area being 400 μm x 1000 μm. In the SSI system, the analysis area is determined by the size of the monochromatic Al x-ray beam on the sample, and the sample is positioned using an optical microscope. Both systems have fast sample insertion capabilities, so analysis can be started about ½ hour after mounting the sample on a holder. The SSI system has a larger sample introduction port allowing samples of 25 mm height to be inserted, whereas this PHI system is limited to samples 15 mm high.

3. Nanowear of ZnO

Zinc oxide thin films can show low friction and long wear life in ambient conditions, and this is thought to be due to extra defects introduced into the ZnO by preferred doping. This concept was tested by a colleague, Jose Nainaparampil, in studying nanowear by the addition of Si (a preferred dopant) into ZnO crystal faces by prolonged scans (tribological stressing) with the Si tip of an atomic force microscope (AFM). Continuous scanning with the Si tip would be expected to form transfer films at the nano-wear scar and produce a reduction in friction. The pyramid tip of the AFM had a height of 3 μm, an apex angle of 15°, and a circular base of 1 μm radius. Lateral force measurements showed that the nanowear scar had a lower friction

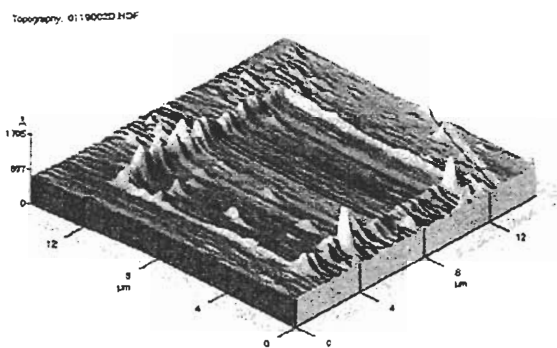

Figure 1. Wear scar formed on ZnO (0001) after scanning 16 – 18 hours with a Si AFM tip. The average depth of the wear scar is 2 nm.

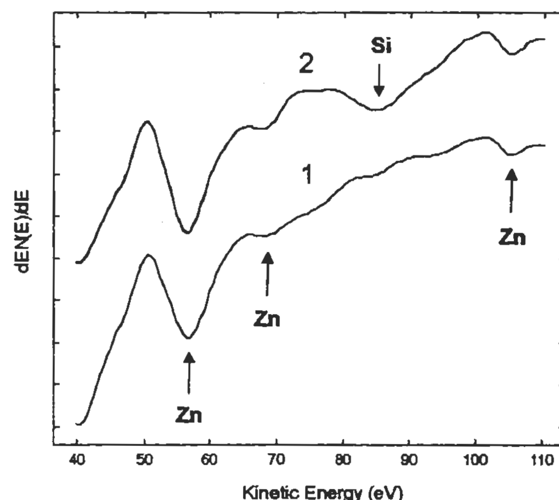

Figure 2. Low energy, derivative Auger spectra from ZnO sample; background area outside the nanowear scar (spectrum 1), and within the nanowear scar (spectrum 2). An 11 nA, 5 keV electron beam was used for analysis.

coefficient than the surrounding areas [1]. AES was used to examine the wear scar for the presence of Si.

Auger spectra were acquired both in the nanowear scar and on the surrounding area, and are shown in Figures 2 and 3. As the worn area could not be seen in an SEM image, the worn area was located by referencing it to a TEM grid. Figure 2 shows the three Zn transitions (40-110 eV) from ZnO in the un-worn surrounding region (spectrum 1). Spectrum number 2 in Figure 2 was taken from the nanowear scar and shows the additional presence of Si. The presence of Si in the nanowear scar was confirmed using the high energy Si, $KL_{2,3}L_{2,3}$ transition as shown in Figure 3, spectrum 2; the spectrum numbered 1 is from the surrounding un-worn area. The spectra shown here are in derivative form and were obtained from the raw data using a 9-point Savitsky-Golay smooth and a 5-point derivative. Auger signals were detected from Zn, O, C, and Si, and their atomic concentrations were calculated from the intensities of the derivative Auger peaks, giving atomic concentrations of 20, 13, 65, and 2%, respectively in the nanowear scar. The corresponding atomic concentrations for Zn, O, and C from the un-worn surrounding area are 19, 11, and 70%, respectively. These calculations assume that the analyzed regions are homogeneous.

An energy dispersive spectroscopy (EDS) study of the worn tip showed the presence of Zn, which came from the ZnO crystal.

In conclusion, prolonged scanning of a Si AFM tip on a ZnO (0001) surface results in a lubricious surface, and AES proved the transfer of Si to the ZnO from the tip. Details of this work can be read in reference [1].

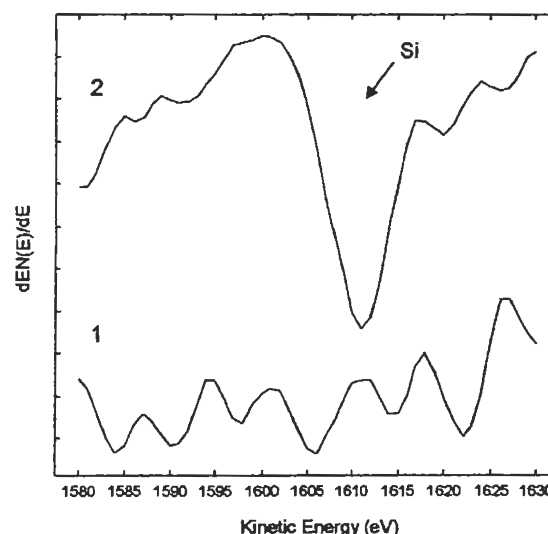

Figure 3. High energy, Si $KL_{2,3}L_{2,3}$ derivative Auger spectra from ZnO sample; background area outside the nanowear scar (spectrum 1), and within the nanowear scar (spectrum 2). An 11 nA, 5 keV electron beam was used for analysis.

4. Al/Ti Films on SiC

A series of Al/Ti films grown on SiC were examined after different annealing temperatures. The goal of this project was to determine if and when interdiffusion between the deposited layers occurred. AES is ideally suited for this study, as sputter depth profiles through the films will show when diffusion occurred. Linear least squared fitting of the spectra also allowed Auger peak overlap problems to be removed, to determine if different chemical states of the elements exist in

the layered structure, and to improve the signal to noise in the profile [2]. Four sets of films were examined, one being unannealed, the others where samples had been annealed at 700, 850, and 1000°C.

For the sputter depth profiles, a 10 nA, 5 keV electron beam was used for Auger electron production, and a 2 mm x 2 mm rastered, 3 keV Ar^+ ion beam was used for sputtering. Auger measurements and sputtering were alternated to prevent complications from ion excited Auger emission within the Al film [3]. Samples were not rotated during sputtering.

The unannealed samples showed no significant interdiffusion between the Al and Ti layers, as can be seen from the profile in Figure 4. A limited number of measurements were made in this profile. Note the presence of an aluminum oxide layer at the surface, and the presence of a few atomic percent O within the Al film.

On the other hand, all the annealed samples showed various degrees of interdiffusion as can be seen in the profiles displayed in Figures 5 - 7.

After annealing at 700°C, significant interdiffusion has occurred. Ti was detected at the surface before sputtering. As soon as the surface carbon contamination is removed (after the first sputtering cycle), the C peak shape (curve C1.ls1) is typical for that of a metal carbide [4], so it appears that titanium carbide is present during the first several minutes of sputtering. The C concentration then decreases significantly, but some titanium carbide is present throughout the remaining Ti containing region. The Al concentration is very low near the surface,

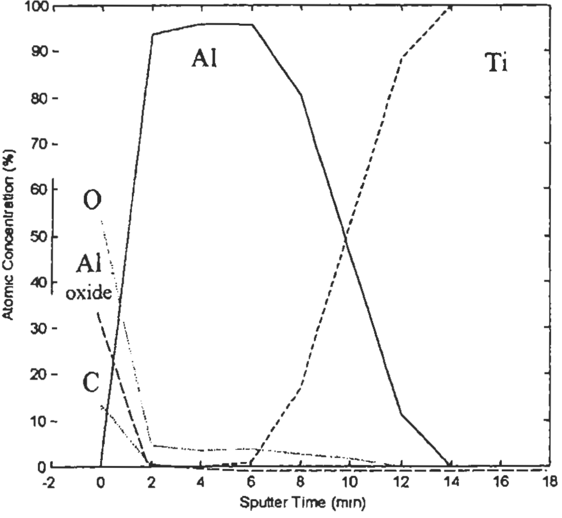

Figure 4. Auger sputter depth profile through an unannealed Al/Ti film structure deposited on GaAs.

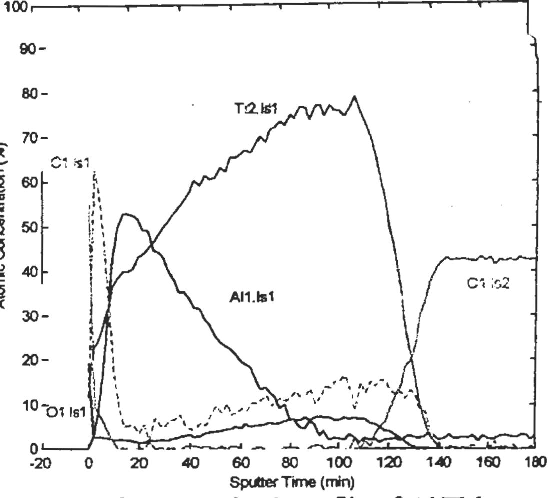

Figure 5. AES sputter depth profile of Al/Ti layers on SiC after annealing at 700°C.

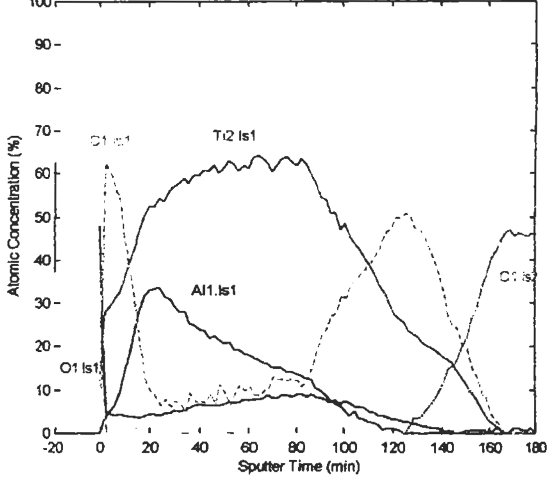

Figure 6. AES sputter depth profile of Al/Ti layers on SiC after annealing at 850°C.

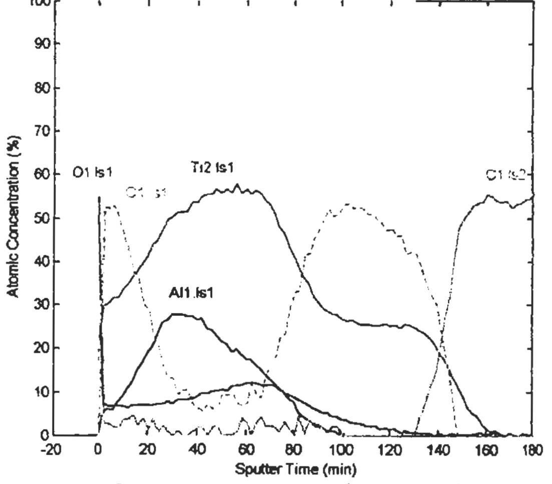

Figure 7. AES sputter depth profile of Al/Ti layers on SiC after annealing at 1000°C.

increases rapidly below the titanium carbide layer, and then decreases within the remaining Ti region.

Oxygen was also detected throughout the Al-Ti region, and dropped to zero within the SiC. The SiC substrate is quite clear, and the C lineshape here (curve C1.ls2) is different from that of a metal carbide and is typical for that from SiC [4].

After annealing at 850°C, Figure 6, significant reaction with the SiC substrate was also observed. The C lineshape is that of metallic carbide (curve C1.ls1) both near the surface and near the SiC substrate. There is also a different Si lineshape (curve Si1.ls1) near the SiC substrate.

The sputter depth profile after annealing at 1000°C, Figure 7, shows further reactions. The carbide layers (curve C1.ls1) appear wider, with a corresponding change in the Ti distribution (curve Ti2.ls1). The Ti Auger transitions used in these profiles are the LMM transitions near 420 eV. Similar profiles were obtained using the LMM transitions near 390 eV. The Al and Si transitions used were the $L_{2,3}VV$.

This analysis shows the usefulness of AES sputter depth profiling to monitor the diffusion of Al/Ti layers on SiC. The information and quality of the profiles was enhanced by linear least squares fitting of the data.

5. MEMS Switch Fabrication

In RF MEMS switch fabrication on GaAs substrates, an unknown white residue was observed after stripping the photoresist. Several pieces of residue could be seen, the largest being about 500 μm in size. When this sample was received the PHI system (for AES analysis) was not available so XPS was performed with the SSI system.

XPS analysis on the largest piece of residue gave surface concentrations of 75 at. % C, 20 at. % O, with the remainder being N (this assumes the surface composition is homogeneous in this region). A region away from the residue gave similar relative concentrations of C, O and N, but with about 0.7 at. % each of Ga and As. This region is known to be non-homogeneous, due to the patterning on the device. This analysis shows that the deposit is thick enough to prevent signal from the GaAs substrate from being detected (as expected) and is probably due to photoresist. However, with the small size of the residue there is some uncertainty in position of the 150 μm x-ray beam on the sample using the microscope for alignment as this system is used by many people for various projects, and an alignment calibration of the microscope was not performed

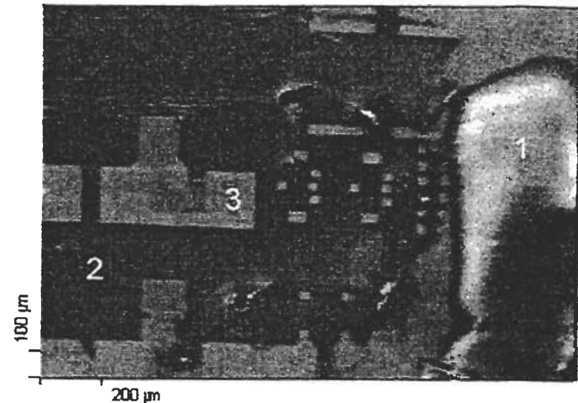

Figure 8. SEM image of RF MEMS switch fabrication on GaAs, showing three regions examined with AES.

just prior to analysis. The sample was then scheduled for later analysis with AES in the PHI system.

With the electron beam in the PHI system, the residue could be easily located. An SEM image from part of the sample is shown in Figure 8, where the deposit appears as the large region (labeled 1) on the right. Note the patterned areas on the sample also. Auger spectra taken from the three marked areas in Figure 8 are shown in Figure 9. Note that the patterned area (labeled 3) shows Ga and As signals from the substrate, whereas the other two areas do not. The C signal from region 1 is broader than that from regions 2 and 3 and indicates charging.

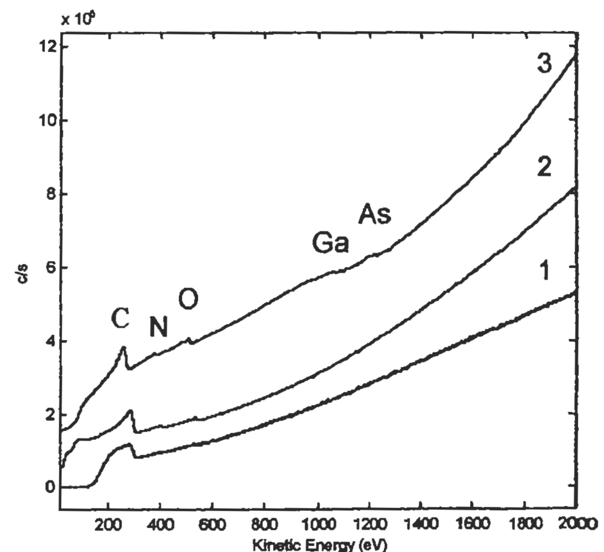

Figure 9. AES spectra from the three regions shown in Figure 8. Region 1 is on the deposit at the right, region 2 is on the background region to the left, and region 3 is a light colored (patterned) area. Spectra are offset for clarity. Spectra were obtained with a 3 nm, 5 keV electron beam.

\ES analysis shows that the residue was with a composition similar to photoresist. te residue occurred due to the apparent)n of photoresist and a low power RF bias sputter cleaning process. The plasma altered the state of the photoresist in reas such that standard photoresist ; solutions did not remove the residue that Based on this analysis, the ıography processing steps have been l to eliminate this problem.

ɩ in Aluminum Aircraft Alloy

vas used to determine the composition at places along a crack in an aluminum l part from an aircraft. The crack was g, about 25 cm, and the part had been cut sections along its length, and cut from o each part was about 2 cm thick. Each vas mounted and analyzed separately. A ph of the crack is shown in Figure 10. was performed at 19 places along the rresponding to parts with different optical .ces. The elements detected, and their ations, are listed in Table 1.

ı be seen from Table 1, Cd, P and Ca were ⁄ detected from the top of the crack, left igure 10, (analysis location 1) down to the ction number 4 (location 14). Mg was on the lower half of the crack, and Al l (generally) down the crack. About 1 percent Zn was detected almost ere on the crack surface (Mg and Zn are n the alloy). Section number 2 showed a ıic percent F at all locations (locations 3 8), but as none was found on the other

Table 1. Atomic concentrations of elements detected at the 19 regions examined along the crack shown in Figure 10. The concentrations are in atomic percent, and assume that the surface is homogeneous within each 400 µm x 1000 µm analysis area.

Location	Zn	O	Ca	C	Al	Cd	N	Mg	Na	Si	S	F	P	Cu	Cl
1	1.1	25	1.1	71		0.7	1.0						0.4		
2	1.0	23	1.5	70	2	0.7	0.8						1.4		
3	0.9	23	1.5	68	2	0.5	0.3					3.0	1.1		
4	1.1	30	1.0	59	5	0.1	0.5					1.5	0.8	0.1	
5	1.4	28	1.9	61	2	0.8	0.1		0.4			3.2	1.7		
6	1.2	24	1.7	68		0.6	0.4					2.5	1.5		
7	1.2	32	2.2	54	4	0.6	0.9					3.5	2.3		
8	1.4	33	2.6	54	4	0.8	0.1					2.1	2.8		
9	1.4	32	1.8	57	4	0.7	0.3						2.7		
10	1.4	31		60	5	0.4	0.6						1.7		
11	0.5	43	1.2	39	15		0.7								
12	0.7	46	2.1	38	13	0.03	0.1	0.0							
13	1.0	48	1.3	36	12	0.09	0.3	1.4					0.4		
14	1.1	39	2.5	47	6	0.3	0.4	0.8		0.9			1.2		
14	1.1	39	2.6	47	7	0.3	0.4	1.3	0.2	0.9	0.3		1.1		
15	0.7	54		17	22			5.9							
16	0.6	43		37	11		0.7	3.8	1.8	1.5	0.6				
17	0.4	42		35	16		0.7	4.9	0.5						
18	0.2	34		49	10		1.3	3.2	0.9	1.5	0.2				
19		30		46	14		1.5	4.3		3.2					0.5

specimens, it was most likely contamination from handling.

This information was given to the client, and it was determined that the Cd was from a fastener at the crack initiation point.

7. Hexamethyldisiloxane Barrier Layers

Polymeric optical materials are of interest in the telecommunications, display, and laser markets, and in some of these applications, organic dyes (chromophores) are added to the polymer host to add linear or nonlinear optical properties to the system. In homogeneous systems, dye diffusion is not an issue. However in stacks of polymer films with different dye concentrations or in films with a spatially varying dye concentration, diffusion becomes important. XPS was used to study the control of dye diffusion in poly(dimethylsiloxane)

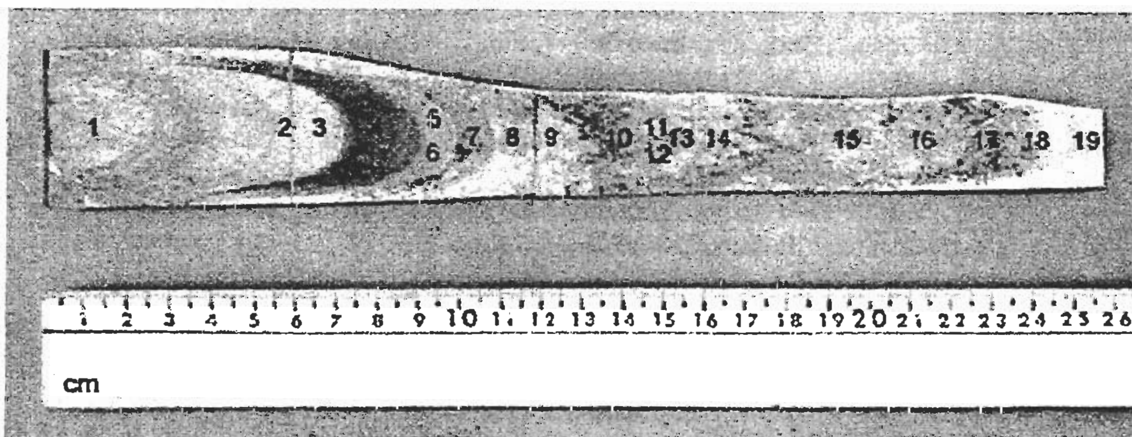

10. Optical micrograph of a long crack in n aircraft alloy, showing the 19 places that ysis was performed. The top of the crack is on

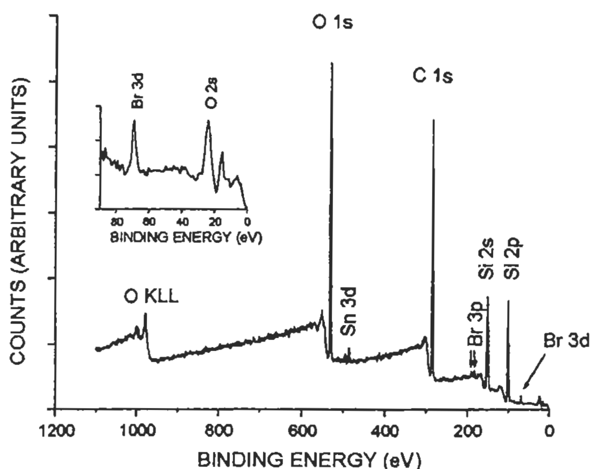

Figure 11. XPS survey spectrum of ZnOBP-doped crosslinked polysiloxane. The bromine 3d peak, occurring near 70 eV as indicated by the arrow, is shown enlarged in the inset. The spectrum took 10 minutes to acquire.

films using barrier layers of hexamethyldisiloxane (HMDS). The dye used was zinc octabromylporpyhrin (ZnOBP), and was doped into the poly(dimethylsiloxane) films. The diffusion barrier layers of HMDS, 60 – 240 nm thick, were deposited between doped and undoped layers of poly(dimethylsiloxane) using plasma enhanced chemical vapor deposition. Diffusion of the chromophore to the outside surface of the undoped layer was examined with and without plasma polymerized barrier layers. Diffusion was monitored by looking for Br on the outer surface of the undoped layer.

An XPS survey scan from the surface of a ZnOBP doped layer is shown in Figure 11. The Br 3d signal near 70 eV binding energy is shown more clearly in the inset. The Sn 3d signal is from a dibutyltin dilaurate catalyst. To improve the detectability of Br, the spectral region for the Br 3d signal was acquired separately for 15 minutes, resulting in a Br detectability limit of 0.02 atomic %.

Figure 12 shows the Br 3d spectral regions obtained from the surfaces of dye-free layers after five days, for barrier layers of 60, 120, 180, and 240 nm thickness, (a) – (d) respectively. Spectrum (e) was taken from a sample without a barrier layer, and (f) was taken from the surface of a dye-doped layer. The lack of a Br 3d peak near 70 eV for the samples with barrier layers, (a) – (d), indicates that the barrier layers were successful in limiting diffusion of the dye. In contrast, a Br 3d peak was observed in the spectrum from the sample without a barrier layer, (e), showing that diffusion of dye through the undoped layer had occurred. All four

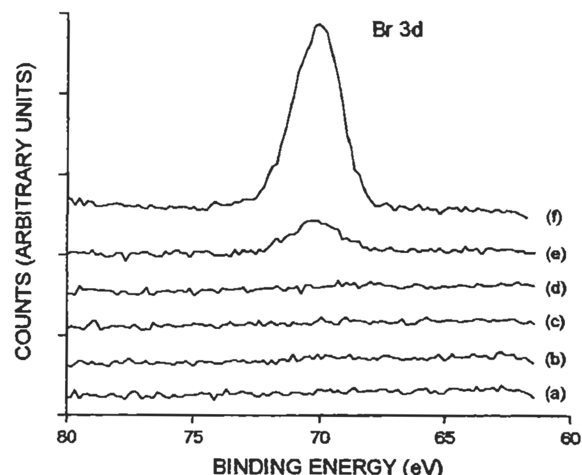

Figure 12. Br 3d XPS spectra from the undoped layer surfaces of five undoped/doped structures, (a) – (d), with plasma polymerized HMDS inter-layers of 60, 120, 180, and 240 nm thickness respectively; a structure without a barrier layer (e); and from the surface of a doped layer as a reference, (f). All spectra were taken 5 days after formation, and each spectrum took 15 minutes to acquire. The spectra have been offset for clarity.

barrier layers thicknesses were found to be effective in limiting diffusion over 5 days.

Studies on longer time scales also indicate that the barrier layer limits diffusion although not completely eliminating it. After three months time, both the 60 nm and 120 nm thick barrier layers allowed enough dye to diffuse between layers to exceed the detection limit of 0.02 atomic % bromine, whereas the 180 and 240 nm barrier layers did not. This longer term study indicates that the thickness of the barrier layer is an important parameter in the long term effectiveness of the barrier layer.

In summary, XPS showed that the use of plasma enhanced chemical vapor deposition to deposit thin barrier layers of hexamethyldisiloxane is a possible methodology to limit or eliminate diffusion of chromophores across interfaces in optical stacks. The thickness of the barrier layer was found to play a role in the diffusion reduction properties of the barrier layer. More details about this project can be read in reference [5].

8. Ce Surface Chemistry

XPS was used to determine the oxidation state of Ce-based conversion coatings that were formed by a spontaneous reaction between a water-based solution containing $CeCl_3$ and aluminum alloy

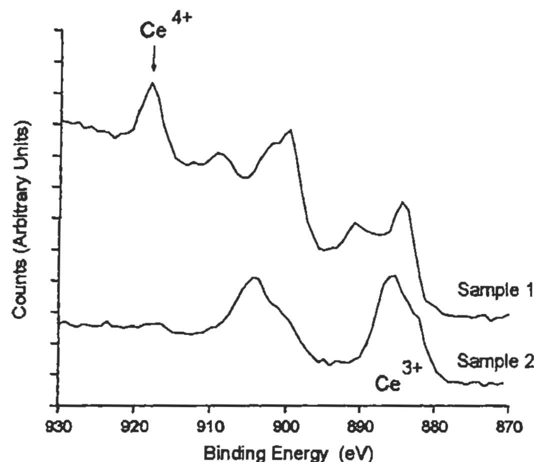

Figure 13. Ce 3d spectra obtained from conversion coatings prepared in two different ways. Sample 1 shows predominantly Ce^{4+}.

substrates. Ce-based coatings are a promising alternative to chromate conversion coatings, which will be severely limited in the future due to the expected high costs of worker protection, air monitoring, and waste disposal. Ce photoelectron spectra are very sensitive to oxidation state. A recent study of Ce dopants in sol-gel coatings included Ce 3d spectra of several Ce containing materials [6]. It has been known for quite some time that Ce^{4+} spectra have strong satellite structure, the most obvious feature being a peak near 918 eV, whereas Ce^{3+} spectra do not [7].

In this work, it was found that the Ce oxidation state in the coatings varied depending on the preparation conditions, but most coatings had predominantly a Ce^{4+} oxidation state. This was rather surprising, since the Ce salt used in making the films was Ce^{3+}. Examples are shown in Figure 13. More details of this work can be read in reference [8].

9. Acknowledgements

The author would like to thank his colleagues for providing these samples for analysis: Jose Nainaparampil for the nanowear of ZnO; Mike Capano for the Al/Ti films on SiC; Kevin Leedy for the MEMS switch fabrication on GaAs; Deb Peeler for the crack in the Al aircraft alloy; Eric Johnson for the hexamethyldisiloxane barrier layers; and Matt O'Keefe for the Ce containing barrier coatings. The support of the U.S. Air Force Research Laboratory in conducting these analyses is also gratefully acknowledged.

10. References

[1] J. J. Nainaparampil, J. T. Grant, and J. S. Zabinski, Wear, in submission.
[2] W. F. Stickle, and D. G. Watson, J. Vac. Sci. Technol. A, 10, 2806 (1992).
[3] J. T. Grant, M. P. Hooker, R. W. Springer, and T. W. Haas, J. Vac. Sci. Technol. 12, 481 (1975).
[4] T. W. Haas, J. T. Grant, and G. J. Dooley, J. Appl. Phys., 43, 1853 (1972).
[5] E. M. Johnson, S. J. Clarson, H. Jiang, W. Su, J. T. Grant, and T. J. Bunning, Polymer 42, 7215 (2001).
[6] L. S. Kasten, J. T. Grant, N. Grebasch, N. Voevodin, F. E. Arnold, and M. S. Donley, Surf. Coat. Trechnol., 140, 11 (2001).
[7] P. Burroughs, A. Hammett, A. F. Orchard, G. Thornton, J. Chem. Soc. Dalton Trans., 1686 (1976).
[8] W. G. Fahrenholtz, M. J. O'Keefe, H. Zhou, and J. T. Grant, Surf. Coat. Trechnol., in press.